
Locality-aware Surrogates for Gradient-based Black-box Optimization

Ali Momeni^{* 1,2} Stefan Uhlich³ Arun Venkitaraman^{1,4} Chia-Yu Hsieh^{1,4} Andrea Bonetti^{1,4} Ryoga Matsuo^{3,2}
Eisaku Ohbuchi⁴ Lorenzo Servadei^{1,4}

Abstract

In physics and engineering, many processes are modeled using non-differentiable black-box simulators, making the optimization of such functions particularly challenging. To address such cases, inspired by the Gradient Theorem, we propose locality-aware surrogate models for active model-based black-box optimization. We first establish a theoretical connection between gradient alignment and the minimization of a Gradient Path Integral Equation (*GradPIE*) loss, which enforces consistency of the surrogate’s gradients in local regions of the design space. Leveraging this theoretical insight, we develop a scalable training algorithm that minimizes the *GradPIE* loss, enabling both offline and online learning while maintaining computational efficiency. We evaluate our approach on three real-world tasks – spanning automated *in silico* experiments such as coupled nonlinear oscillators, analog circuits, and optical systems – and demonstrate consistent improvements in optimization efficiency under limited query budgets. Our results offer dependable solutions for both offline and online optimization tasks where reliable gradient estimation is needed.

1. Introduction

Optimizing black-box objective functions over large design spaces is a major challenge in many scientific and engineering fields. Examples include designing molecules, proteins, drugs, biological sequences, and materials (Sarkisyan et al., 2016; Nguyen & Daugherty, 2005; Si et al., 2016; Ashby, 2000). Although several approaches, such as genetic algorithms (Banzhaf et al., 1998) and Bayesian optimization (BayOpt) (Shahriari et al., 2015), are commonly used

for non-differentiable black-box optimization, we focus on gradient-based optimization due to its scalability and efficiency. One common approach is to train a differentiable surrogate model on given data to approximate the objective function value (or its inverse) for unknown inputs. Once trained, we can perform gradient ascent on the input space to find the best input points (Kumar & Levine, 2020; Brookes et al., 2019; Hutter et al., 2011). This *in silico* method, known as offline model-based black-box optimization, simplifies the optimal design problem into a straightforward application of supervised learning and gradient ascent, without actively querying the black-box function during optimization. A key assumption of this approach is that an “accurate” surrogate model can be learned across the entire input space, which is often not possible due to the limited offline training data. The forward model (here a surrogate model) may incorrectly assign high scores to points outside the training data range (Krishnamoorthy et al., 2022). These inaccurate predictions can mislead the optimization process toward sub-optimal candidates. Several solutions have been proposed, mainly focusing on adding conservative preferences to the search or surrogate training process (Trabucco et al., 2021; Kumar & Levine, 2020; Fannjiang & Listgarten, 2020; Chemingui et al., 2024; Dao et al., 2024). For example, Conservative Objective Models (COMs) (Trabucco et al., 2021) address this issue by penalizing high scores for out-of-dataset points, but this can also prevent exploration of high-quality points far from the training data.

On the other hand, *active black-box optimization* (ABBO) addresses the issue of unreliable forward model predictions for out-of-distribution offline data by allowing the querying of the black-box function during the forward pass. Recently, stochastic gradient estimators (Mohamed et al., 2020), such as the REINFORCE estimator (Williams, 1992), have been employed to estimate gradients of non-differentiable functions, enabling gradient-based optimization. To use the strengths of gradient-based optimization and mitigating the high variance often associated with score function gradient estimators, a recent approach involves training a surrogate model as before but using it exclusively in the backward pass to estimate the gradient of the objective function with respect to the inputs (Shirobokov et al., 2020; Grathwohl et al., 2017). This approach is suitable for various black-box

Work done during an internship at SonyAI. ¹SonyAI, Switzerland ²EPFL, Switzerland ³Sony Semiconductor Solutions Europe, Germany ⁴Sony Semiconductor Solutions, Japan. Correspondence to: Ali Momeni <ali.momeni@epfl.ch>.

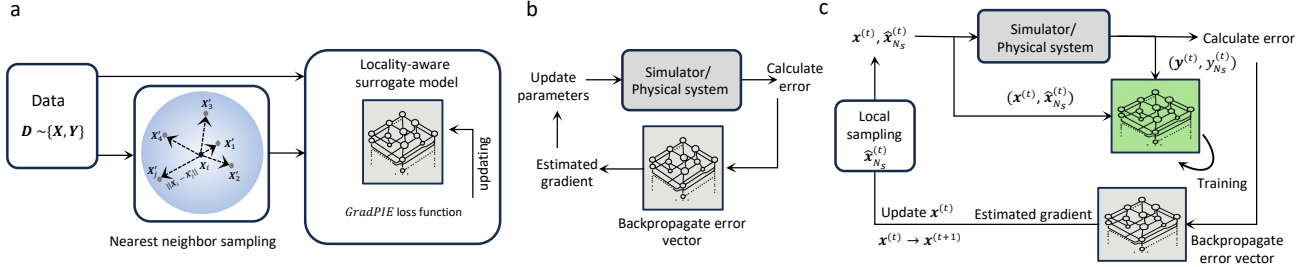


Figure 1. **a** Our method calculates the k -nearest neighbors for each sample in the dataset. These neighbors are used to train the locality-aware surrogate model with the *GradPIE* loss function. **b** Active black-box optimization (ABBO) using the surrogate model trained offline. **c** ABBO with online training of the surrogate model.

optimization problems where automated querying of the black-box function is possible, typically in automated *in silico* or *in situ* experimental settings, such as simulators (Shiobokov et al., 2020), physical systems (Wright et al., 2022), robotics (de Avila Belbute-Peres et al., 2018; Degraeve et al., 2019), and smart sensors (Zhou & Chai, 2020; Mennel et al., 2020). Additionally, this technique has recently been experimentally applied to the training of physical neural networks (analog neural networks), as shown in (Wright et al., 2022; Zheng et al., 2023; Spall et al., 2022; Oguz et al., 2024; Momeni et al., 2023a). In this case, the overall effectiveness of the optimization loop depends on how accurately the surrogate model can estimate the gradient under limited query budgets. This leads to an important question: how can we train such surrogate models to achieve more accurate gradient estimation within the same query budgets?

In this paper, inspired by the gradient theorem (Williamson & Trotter, 2004), we propose *locality-aware* surrogate models for ABBO. The main contributions of this work are:

1— To address the question mentioned earlier, we first theoretically demonstrate that minimizing the *GradPIE* loss—derived from the Gradient Theorem—ensures alignment between the gradients of the surrogate model and the black-box function. This theoretical result is validated experimentally on a Coupled Nonlinear Oscillator Network, used as a toy example.

2— We propose a scalable training algorithm for locality-aware surrogate models to minimize the *GradPIE* loss. This algorithm supports both, offline training (leveraging pre-collected datasets) and online adaptation (refining gradients iteratively during optimization), ensuring computational efficiency even in high-dimensional design spaces.

3— We evaluate our framework on three real-world tasks—spanning automated *in silico* experiments (e.g., simulators) and physical systems—where automatic querying of black-box functions is feasible. Our results demonstrate consistent improvements in optimization performance under limited query budgets compared to traditional methods.

2. Background and Problem Setup

Black-box Optimization. Suppose $\mathfrak{X} \in \mathbb{R}^{D_i}$ is an input space, and each $\mathbf{x} \in \mathfrak{X}$ is a candidate input. Let $\mathbf{F} : \mathfrak{X} \rightarrow \mathbb{R}^{D_o}$ represent the black-box system (simulator or physical system) that maps any input $\mathbf{x} \in \mathfrak{X}$ to an output $\mathbf{y} = \mathbf{F}(\mathbf{x})$. Also, let $\psi : \mathbb{R}^{D_o} \rightarrow \mathbb{R}$ be an objective function that gives a real value. In general, the goal is to find an optimal input $\mathbf{x}^* \in \mathfrak{X}$ that maximizes the objective function associated with the output of the black-box system $\mathbf{F}(\mathbf{x})$, i.e.,

$$\mathbf{x}^* \triangleq \arg \max_{\mathbf{x} \in \mathfrak{X}} \psi(\mathbf{F}(\mathbf{x})). \quad (1)$$

We are given a dataset consisting of N input-output pairs $\mathcal{D} = \{(\mathbf{x}_1, \mathbf{y}_1), (\mathbf{x}_2, \mathbf{y}_2), \dots, (\mathbf{x}_N, \mathbf{y}_N)\}$, where each $\mathbf{y}_i = \mathbf{F}(\mathbf{x}_i)$ is the output of the black-box system \mathbf{F} .

Surrogate model (Base-model). We focus on an optimization scheme that uses the black-box system (simulator or physical system) in the forward pass of the optimization loop and a pre-trained surrogate model in the backward pass (see Fig. 1b). The role of the pre-trained surrogate model is to estimate the gradient of the black-box system’s output with respect to the input.

We can train a surrogate model $\hat{\mathbf{F}}(\mathbf{x}; \boldsymbol{\theta})$ using the dataset \mathcal{D} to approximate $\mathbf{F}(\mathbf{x})$ through supervised learning.

$$\boldsymbol{\theta} \triangleq \arg \min_{\boldsymbol{\theta}'} \sum_{i=1}^N \mathcal{L}(\hat{\mathbf{F}}(\mathbf{x}_i; \boldsymbol{\theta}'), \mathbf{y}_i) \quad (2)$$

where $\boldsymbol{\theta}$ represents the parameters of the surrogate model, and \mathcal{L} is the loss of predicting $\hat{\mathbf{F}}(\mathbf{x}; \boldsymbol{\theta})$ when the true output is \mathbf{y} for a given input \mathbf{x} .

ABBO using offline training of the surrogate model. As mentioned earlier, the surrogate model can be trained offline. In this approach, the surrogate model is first trained on a fixed \mathcal{D} and then used during the backward pass of the optimization loop (see Fig. 1b and Algorithm A1).

ABBO using online training of the surrogate model. Another approach involves training the surrogate model in an online manner. In this method, during each iteration of the optimization process, the surrogate model updates itself with new input data (optionally incorporating N_s local samples).

After updating, the surrogate model is used in the backward pass to estimate the gradients (see Fig. 1c and Algorithm 1). To retrain the surrogate model effectively, a local sampling scheme is used. This scheme generates N_s samples from a normal distribution with a small standard deviation centered around the updated solution, $\mathbf{x}(t+1)$. This localized sampling strategy with simple rank selection process improves the surrogate model’s ability to accurately capture the local behavior of the objective function, enhancing optimization performance. Unlike the offline scheme, which requires many input-output pairs to cover the entire landscape of the black-box function, this approach focuses only on the optimization path, making it more efficient in terms of the total number of queries to the black-box function.

3. Theoretical analysis

The performance of the optimization scheme shown in Fig. 1b and 1c strongly depends on how accurately the gradient of the black-box system’s output is approximated with respect to the input. A naïve approach involves sampling perturbed values around a target input and using the finite difference method to approximate its gradient. However, this method requires multiple queries to the black-box function for perturbed data points, thereby increasing the total number of input-output evaluations. Instead, we propose to improve gradient estimation performance by training a locality-aware surrogate model without increasing the total number of input-output pairs. We leverage the gradient theorem (Williamson & Trotter, 2004), which states that for a differentiable function \mathbf{F} and any curve $\gamma_{\mathbf{x}, \mathbf{x}'}$ starting at \mathbf{x} and ending at \mathbf{x}' , we have

$$\int_{\gamma_{\mathbf{x}, \mathbf{x}'}} \nabla \mathbf{F}(\mathbf{r}) \cdot d\mathbf{r} = \mathbf{F}(\mathbf{x}') - \mathbf{F}(\mathbf{x}). \quad (3)$$

To incorporate a learnable model, we replace $\mathbf{F}(\mathbf{x})$ inside the integral with $\hat{\mathbf{F}}(\mathbf{x}; \boldsymbol{\theta})$ —a surrogate model—while retaining \mathbf{F} on the right-hand side of (3). Under this substitution, the equality becomes an approximation, which holds when $\nabla \hat{\mathbf{F}}(\mathbf{x}; \boldsymbol{\theta})$ closely estimates $\nabla \mathbf{F}$. To enforce this, we therefore need to find $\boldsymbol{\theta}$ such that the averaged difference between the LHS and RHS of (3) is minimized which is expressed through the loss function

$$\mathcal{L}_{\text{GradPIE}}(\boldsymbol{\theta}) = E_{(\mathbf{x}, \mathbf{x}') \sim \mathcal{D}^2} \left[\left\| \int_{\gamma_{\mathbf{x}, \mathbf{x}'}} \nabla \hat{\mathbf{F}}(\mathbf{r}; \boldsymbol{\theta}) \cdot d\mathbf{r} - (\mathbf{F}(\mathbf{x}') - \mathbf{F}(\mathbf{x})) \right\|_1 \right], \quad (4)$$

It measures the discrepancy between the integral of the gradient of $\hat{\mathbf{F}}(\mathbf{x}; \boldsymbol{\theta})$ over the path from \mathbf{x} to \mathbf{x}' and the difference in the target values $\mathbf{F}(\mathbf{x}') - \mathbf{F}(\mathbf{x})$. We can further simplify the above loss function into the following form by applying the gradient theorem once more to $\hat{\mathbf{F}}(\mathbf{x}; \boldsymbol{\theta})$

Algorithm 1 Gradient-based Black-box Optimization via Online Training of the Surrogate Model Using *GradPIE*.

Input: Initial surrogate parameters $\boldsymbol{\theta}$, learning rates η_1 and $\eta_2 > 0$, number of epochs L_{epochs} , number of nearest neighbors K , black-box $\mathbf{F}(\cdot)$, number of optimization steps τ , number of local samples N_s , standard deviation σ , number of top samples N_{best} , convergence threshold ϵ

Output: Optimized input \mathbf{x}^*

Initialize: $\boldsymbol{\theta}^{(0)} \leftarrow \boldsymbol{\theta}$ Dataset $\mathcal{D}^{(0)} = \{(\mathbf{x}_i, \mathbf{F}(\mathbf{x}_i))\}_{i=1}^{N_{\text{init}}}$, where $\mathbf{x}_i \sim \mathcal{N}(0, I)$. Precompute \mathbf{x}'_k for each $\mathbf{x}_i \in \mathcal{D}^{(0)}$

for $t = 1$ **to** $\tau - 1$ **do**

// Generate N_s new samples around $\mathbf{x}^{(t)}$ (local sampling)

$\hat{\mathbf{x}}_i^{(t)} \sim \mathcal{N}(\mathbf{x}^{(t)}, \sigma^2 \mathbf{I}_d)$, $i = 1, 2, \dots, N_s$

// Update dataset with new samples

$\mathcal{D}^{(t+1)} \leftarrow \mathcal{D}^{(t)} \cup \{\hat{\mathbf{x}}_i^{(t)}, \mathbf{F}(\hat{\mathbf{x}}_i^{(t)})\}$

Re-train surrogate model:

for $l = 1$ **to** $L_{\text{epochs}} - 1$ **do**

foreach mini-batch $\mathcal{B} \subseteq \mathcal{D}^{(t+1)}$ **do**

| Compute $\mathcal{L}_{\text{GradPIE}}$ using Eq. (10) for \mathcal{B}

end

$\boldsymbol{\theta}^{(l+1)} \leftarrow \boldsymbol{\theta}^{(l)} - \eta_1 \nabla_{\boldsymbol{\theta}} \mathcal{L}_{\text{GradPIE}}(\boldsymbol{\theta})|_{\boldsymbol{\theta}=\boldsymbol{\theta}^{(l)}}$ // Update surrogate parameters

if $\mathcal{L}_{\text{GradPIE}} < \epsilon$ **then**

| **Break** // Stop training if loss converges

end

end

Rank selection: // Select top N_{best} samples

Sort $\mathbf{F}(\hat{\mathbf{x}}_i^{(t)})$ in descending order and select top N_{best} samples

$\mathbf{x}^{(t+1)} \leftarrow \mathbf{x}^{(t)} - \eta_2 \nabla_{\mathbf{x}} \hat{\mathbf{F}}(\mathbf{x}; \boldsymbol{\theta})|_{\mathbf{x}=\mathbf{x}^{(t)}}$ // Update \mathbf{x} using surrogate gradients

end

Return: optimized input \mathbf{x}^* .

yielding

$$\mathcal{L}_{\text{GradPIE}}(\boldsymbol{\theta}) = E_{(\mathbf{x}, \mathbf{x}') \sim \mathcal{D}^2} \left[\left\| (\hat{\mathbf{F}}(\mathbf{x}'; \boldsymbol{\theta}) - \hat{\mathbf{F}}(\mathbf{x}; \boldsymbol{\theta})) - (\mathbf{F}(\mathbf{x}') - \mathbf{F}(\mathbf{x})) \right\|_1 \right]. \quad (5)$$

We will refer to this loss as *GradPIE* loss. In the following, we demonstrate that it learns a superior gradient surrogate compared to the standard mean absolute error (MAE) loss

$$\mathcal{L}_{\text{MAE}}(\boldsymbol{\theta}) = E_{\mathbf{x} \sim \mathcal{D}} \left[\left\| \hat{\mathbf{F}}(\mathbf{x}; \boldsymbol{\theta}) - \mathbf{F}(\mathbf{x}) \right\|_1 \right]. \quad (6)$$

When comparing (5) and (6), we observe that *GradPIE* is invariant to a global offset in $\mathbf{F}(\mathbf{x})$ and $\hat{\mathbf{F}}(\mathbf{x}; \boldsymbol{\theta})$, such as $\mathbf{F}(\mathbf{x}) + \boldsymbol{\mu}_1$ and $\hat{\mathbf{F}}(\mathbf{x}; \boldsymbol{\theta}) + \boldsymbol{\mu}_2$. This is a reasonable property, as our primary goal is to ensure that the gradients are similar to improve utility for optimization. It is important to emphasize that *GradPIE* achieves more than simply removing, for example, the global mean from \mathbf{F} and $\hat{\mathbf{F}}$. As we will discuss later, *GradPIE* is computed locally, ensuring that the learned surrogate $\hat{\mathbf{F}}$ preserves the same relative relationships among function values as observed in \mathbf{F} . This feature enables the learning of a better gradient surrogate. Finally, note that instead of MAE, a mean squared error (MSE) formulation could have been used, which would yield similar results as discussed in this paper.

We now demonstrate that the *GradPIE* loss in (5) minimizes the difference of the Jacobians $\mathbf{J}[\mathbf{F}] \in \mathbb{R}^{D_o \times D_i}$ and $\mathbf{J}[\hat{\mathbf{F}}] \in \mathbb{R}^{D_o \times D_i}$, requiring only paired samples $(\mathbf{x}_i, \mathbf{F}(\mathbf{x}_i))$ for training. By applying the gradient theorem, (5) can be

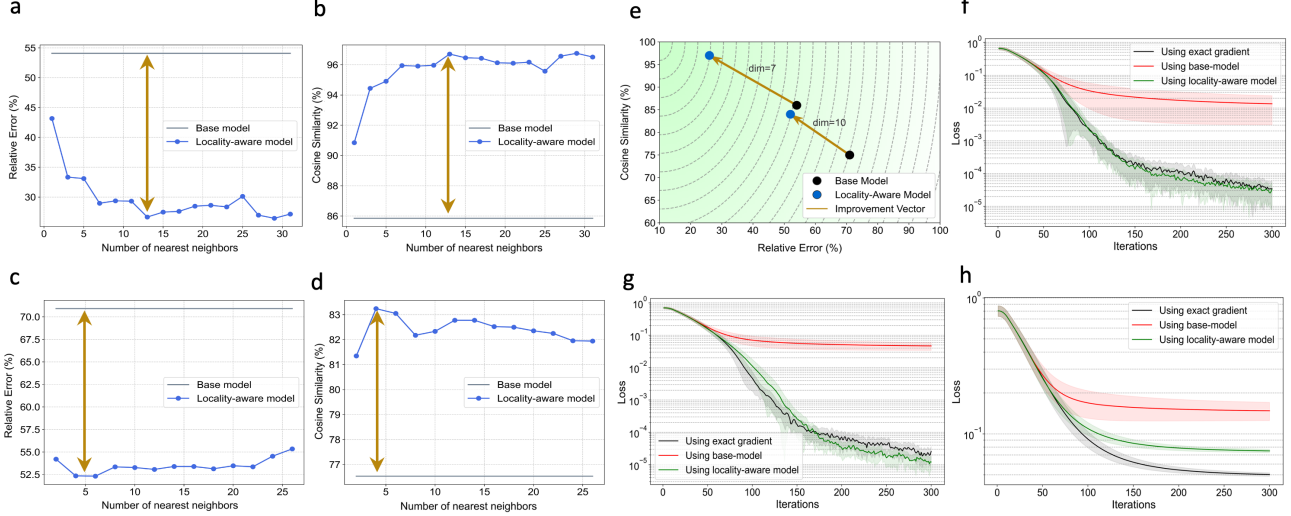


Figure 2. Relative error and cosine similarity between estimated and exact gradient for input dimensions of $D_i = 7$ (a and b) and $D_i = 10$ (c and d), as a function of the number of nearest neighbors for CNON. e The improvement in gradient estimation for optimal number of nearest neighbors. Performance of ABBO using the offline-trained surrogate model for the CNON task for f $\lambda = 0.50$, g $\lambda = 0.55$, and h $\lambda = 0.70$.

rewritten as

$$\mathcal{L}_{\text{GradPIE}}(\theta) = E_{\gamma_{\mathbf{x}, \mathbf{x}'}} \left[\left\| \int_{\gamma_{\mathbf{x}, \mathbf{x}'}} (\mathbf{J}[\hat{\mathbf{F}}](\mathbf{u}; \theta) - \mathbf{J}[\mathbf{F}](\mathbf{u})) d\mathbf{u} \right\|_1 \right], \quad (7)$$

where $\gamma_{\mathbf{x}, \mathbf{x}'}$ is a differentiable curve connecting \mathbf{x} and \mathbf{x}' . For simplicity, we fix \mathbf{x} and assume $\|\mathbf{x} - \mathbf{x}'\| \leq \epsilon$, focusing on (7) for close samples. Under these conditions, the integral can be approximated as

$$\int_{\gamma_{\mathbf{x}, \mathbf{x}'}} (\mathbf{J}[\hat{\mathbf{F}}](\mathbf{u}; \theta) - \mathbf{J}[\mathbf{F}](\mathbf{u})) d\mathbf{u} \approx (\mathbf{J}[\hat{\mathbf{F}}](\mathbf{x}; \theta) - \mathbf{J}[\mathbf{F}](\mathbf{x})) (\mathbf{x}' - \mathbf{x}) \quad (8)$$

and this transforms (7) into

$$\begin{aligned} \mathcal{L}_{\text{GradPIE}}(\theta) &\approx \int_{\|\mathbf{x} - \mathbf{x}'\| \leq \epsilon} \left\| (\mathbf{J}[\hat{\mathbf{F}}](\mathbf{x}; \theta) - \mathbf{J}[\mathbf{F}](\mathbf{x})) (\mathbf{x}' - \mathbf{x}) \right\|_1 p(\mathbf{x}, \mathbf{x}') d\mathbf{x}' \\ &\approx \frac{2\pi^{\frac{N-1}{2}} \epsilon^{N+1}}{(N+1)\Gamma(\frac{N-1}{2} + 1)} p(\mathbf{x}, \mathbf{x}) \left\| \mathbf{J}[\hat{\mathbf{F}}](\mathbf{x}; \theta) - \mathbf{J}[\mathbf{F}](\mathbf{x}) \right\|^{\text{row}} \end{aligned} \quad (9)$$

as $\int_{\|\mathbf{u}\| \leq \epsilon} \mathbf{a}^T \mathbf{u} d\mathbf{u} = \frac{2\pi^{\frac{N-1}{2}} \epsilon^{N+1}}{(N+1)\Gamma(\frac{N-1}{2} + 1)} \|\mathbf{a}\|$ with $\Gamma(\cdot)$ denoting the gamma function and assuming that $p(\mathbf{x}, \mathbf{x}')$ is continuous. Furthermore, we used $\|\mathbf{A}\|^{\text{row}}$ to denote the sum of the 2-norms of all rows of \mathbf{A} , i.e., $\|\mathbf{A}\|^{\text{row}} = \sum_{d=1}^{D_o} \|\mathbf{A}_d\|$. Hence, from (9) we can conclude that minimizing the *GradPIE* loss in (5) corresponds to minimizing the difference between the Jacobians of \mathbf{F} and $\hat{\mathbf{F}}$.

4. Scalable Algorithm: Locality-aware surrogate model

A naïve computation of (5) requires iterating over all pairs of training inputs, which is computationally expensive. To reduce this overhead, we use the k -nearest neighbors for each sample instead. Given the dataset \mathcal{D} , we first compute the k -nearest neighbors for each sample \mathbf{x} (see Fig. 1a) and then calculate following loss during training:

$$\mathcal{L}_{\text{GradPIE}}(\theta) = E_{\mathbf{x} \sim \mathcal{D}} \left[\frac{1}{K} \sum_{k=1}^K \left\| (\mathbf{F}(\mathbf{x}) - \mathbf{F}(\mathbf{x}'_k)) - (\hat{\mathbf{F}}(\mathbf{x}; \theta) - \hat{\mathbf{F}}(\mathbf{x}'_k; \theta)) \right\|_1 \right], \quad (10)$$

where \mathbf{x}'_k represents the k -th nearest neighbor of \mathbf{x} . In the next section, we will empirically show how varying the number of nearest neighbors affects the accuracy of gradient estimation. We will refer to models trained with the GradPIE loss (10) as *locality-aware* models. Algorithm 1 and A1 give the algorithmic description of how we train them.

The advantage of our approach, compared to numerical gradient estimation, lies in the ability of deep surrogate models to capture more complex approximations of the objective function gradient than a linear approximation, making them particularly effective for surfaces with high curvature. Employing such deep neural networks as surrogate models also offers further benefits, such as Hessian estimation for second-order optimization algorithms, uncertainty quantification, and the potential for automatic identification of low-dimensional parameter manifolds.

Locality-aware Surrogates for Gradient-based Black-box Optimization

(1) CNON Task						
Method	$N_s = 0$			$N_s = 1$		
	50 iter	100 iter	200 iter	50 iter	100 iter	200 iter
Exact gradient	0.101 ± 0.013	0.057 ± 0.003	0.048 ± 0.001	0.085 ± 0.017	0.054 ± 0.004	0.048 ± 0.001
Base-model	0.261 ± 0.023	0.188 ± 0.044	0.131 ± 0.041	0.194 ± 0.029	0.151 ± 0.026	0.114 ± 0.030
Locality-aware model	0.198 ± 0.025	0.124 ± 0.031	0.081 ± 0.015	0.186 ± 0.016	0.093 ± 0.013	0.066 ± 0.007
(2) OpAmp Task						
Method	Mean ± Std			IQR: Median (25–75%)		
	50 iter	100 iter	200 iter	50 iter	100 iter	200 iter
Random	7.074 ± 0.904	7.330 ± 0.849	7.628 ± 0.835	7.036 (6.384–7.701)	7.330 (6.714–7.902)	7.610 (7.032–8.224)
Base-model	8.419 ± 1.010	8.628 ± 0.947	8.860 ± 0.899	8.460 (7.785–9.096)	8.689 (8.058–9.311)	8.966 (8.329–9.499)
Locality-aware model	9.011 ± 0.828	9.389 ± 0.727	9.615 ± 0.694	9.068 (8.582–9.473)	9.430 (9.053–9.763)	9.700 (9.292–9.952)
(3) OWMS Task						
Method	Mean ± Std			IQR: Median (25–75%)		
	50 iter	100 iter	200 iter	50 iter	100 iter	200 iter
Random	0.239 ± 0.012	0.233 ± 0.009	0.227 ± 0.009	0.236 (0.232–0.249)	0.235 (0.229–0.238)	0.231 (0.221–0.235)
BayOpt	0.147 ± 0.023	0.120 ± 0.020	0.103 ± 0.019	0.142 (0.133–0.155)	0.119 (0.109–0.129)	0.104 (0.093–0.114)
Base-model	0.172 ± 0.018	0.140 ± 0.015	0.117 ± 0.013	0.172 (0.159–0.186)	0.142 (0.132–0.150)	0.118 (0.109–0.125)
Locality-aware model	0.133 ± 0.014	0.107 ± 0.016	0.090 ± 0.015	0.132 (0.123–0.142)	0.105 (0.095–0.118)	0.087 (0.078–0.102)

Table 1. Performance of ABBO using the online-trained surrogate model across three tasks: CNON, OpAmp, and OWMS. For the CNON task, results are shown for $N_s = 0$ and $N_s = 1$. For the OpAmp and OWMS tasks, we report both the mean ± standard deviation and the median with interquartile range (IQR) at 50, 100, and 200 iterations. Note that smaller values indicate better performance for CNON and OWMS, while larger values indicate better performance for the OpAmp task.

5. Experiments

This section outlines the tasks used to compare the performance of the proposed locality-aware surrogate models with baseline models. Our empirical studies were conducted on three tasks from different engineering domains:

1. **Coupled Nonlinear Oscillator Network (CNON):** We used Coupled Nonlinear Oscillators—dynamic systems defined by nonlinear interactions between oscillatory components (Wright et al., 2022; Lanthaler et al., 2024)—to assess gradient estimation performance compared to the exact gradient. ABBO optimization using offline and online training of the surrogate model experiments was conducted to benchmark results against the ideal scenario with direct access to the exact gradient.
2. **Analog Integrated Circuits (operational amplifier: OpAmp):** The second task involves optimizing a two-stage operational amplifier (OpAmp) circuit by maximizing a figure-of-merit (FOM), which is defined as a combination of open-loop gain, unity-gain bandwidth, and phase margin.
3. **Optical Wave Manipulation System (OWMS):** The final task involves spatial wavefront shaping through the optimization of Spatial Light Modulator (SLM) phase patterns in an optical system (Filipovich & Lvovsky, 2024). The optimization is defined over a 3600-dimensional continuous search space.

5.1. CNON

To empirically evaluate the effectiveness of the proposed *GradPIE* loss function, we start with a toy example: a Cou-

pled Nonlinear Oscillator Network (CNON) described by the following equations of motion

$$\frac{d^2 \mathbf{q}_i}{dt^2} = -\sin(\pi \mathbf{q}_i) + \sum_{j=1}^N \tilde{\mathcal{J}}_{ij} (\sin(\pi \mathbf{q}_j) - \sin(\pi \mathbf{q}_i)) + \boldsymbol{\epsilon}_i, \quad (11)$$

where \mathbf{q}_i are the oscillator amplitudes, $\tilde{\mathcal{J}}_{ij}$ are the symmetric coupling coefficients, and $\boldsymbol{\epsilon}_i$ are the individual oscillator drives. Eq. (11) is often used as approximation to represent the Frenkel-Kontorova model, a widely used model in condensed matter physics (Braun & Kivshar, 1998; Wright et al., 2022).

We encode the input data as the initial amplitudes, \mathbf{q}_i^0 , and take the output to be the state of the oscillator after some time evolution, \mathbf{q}_i^∞ (see Appendix for details).

To evaluate the effectiveness of gradient estimation, we train a multilayer neural network using two loss functions: \mathcal{L}_{MAE} and $\mathcal{L}_{\text{GradPIE}}$, with a dataset containing $N = 1000$ input-output pairs. We then assess the performance of gradient estimation by calculating the relative error, $\text{Relative Error} = \frac{\|\mathbf{g}_{\text{est}} - \mathbf{g}_{\text{exact}}\|}{\|\mathbf{g}_{\text{exact}}\|}$, and the cosine similarity, $\cos(\theta) = \frac{\mathbf{g}_{\text{est}} \cdot \mathbf{g}_{\text{exact}}}{\|\mathbf{g}_{\text{est}}\| \|\mathbf{g}_{\text{exact}}\|}$, between the estimated gradient vector, \mathbf{g}_{est} , and the exact gradient vector, $\mathbf{g}_{\text{exact}}$.

The relative error and cosine similarity for dimensions $D_i = 7$ and $D_i = 10$ as a function of the number of nearest neighbors are shown in Figs. 2a and b and Figs. 2c and d, respectively. As illustrated, the *GradPIE* loss significantly improves gradient estimation performance. This improvement is reflected in relative error reductions of over 27% and 20%, and cosine similarity increases of more than 10% and 8%, respectively. In this experiment, increasing the number

of nearest neighbors does not necessarily lead to improved performance. The optimal value of this parameter is highly correlated with the dimensionality and complexity of the problem, making it a case-dependent hyperparameter. In Fig. 2e, we summarize the improvement in gradient estimation in terms of relative error (x-axis) and cosine similarity (y-axis) for the optimal number of nearest neighbors.

We perform ABBO optimization using offline training of the surrogate model for a CNON with a dimensionality of $D_i = 7$. The optimization problem is defined as

$$\mathbf{q}^{0*} \triangleq \arg \min_{\mathbf{q}^0} \|\mathbf{q}^\infty - \boldsymbol{\lambda}\|_1, \quad (12)$$

where \mathbf{q}^0 and \mathbf{q}^∞ represent the initial and final states of the oscillator amplitude vectors, respectively. \mathbf{q}^{0*} denotes the optimal initial state of the oscillator amplitude vector, and $\boldsymbol{\lambda}$ is a fixed target vector. The goal is to minimize the $\ell_{1\text{-norm}}$ of the deviation between \mathbf{q}^∞ and $\boldsymbol{\lambda}$, ensuring the system converges to the desired configuration. The surrogate model is initially trained on a dataset consisting of $N = 1000$ input-output pairs. Once trained, the model is used within a gradient-based optimization scheme (illustrated in Fig. 1b) to evaluate its performance across three different cases: the base model, the locality-aware model, and a baseline case using the exact gradient for comparison. Figures 2f–h present the results for three distinct values of $\boldsymbol{\lambda}$. The plots clearly show the superior performance of the locality-aware model compared to the base model, demonstrating the effectiveness of incorporating the *GradPIE* loss function in improving optimization performance.

An ABBO optimization using online training of the surrogate model is also implemented for a CNON with a dimensionality of $D_i = 10$. In this framework, the surrogate model is iteratively updated during the gradient-based optimization loop using newly updated input-output pairs. Once updated, the surrogate model is frozen and used to estimate gradients in subsequent iterations. The results for $N_s = 0$ and $N_s = 1$, covering three scenarios - using the exact gradient, the baseline model, and the locality-aware model (with the *GradPIE* loss function) - are shown in Figs. 3a and b, respectively. A quantitative comparison of the different methods' performance at 50, 100, and 200 iterations is provided in Table 1. In both cases, the locality-aware model outperforms the base model and closely approaches the performance achieved using the exact gradient. For $N_s = 1$, the optimization performance aligns more closely with the exact gradient case, especially after the 100th iteration. This improvement is attributed to the inclusion of the local sampling scheme.

5.2. OpAmp

As a second task, we explore the use of ABBO optimization for sizing a two-stage OpAmp circuit, as shown in

Fig. 3c. Specifically, the problem involves sizing the length and width of the MOSFET transistors and the value of a capacitor, resulting in an optimization problem with $D = 10$ variables. The goal is to maximize the figure of merit (FoM):

$$\text{FoM} = 1.2 \cdot \frac{G}{100} + 1.6 \cdot \frac{\text{PM}}{90^\circ} + 10 \cdot \frac{\text{UGBW}}{1 \text{ GHz}} \quad (13)$$

where G denotes the linear DC gain, PM the phase margin in degrees, and UGBW the unity-gain bandwidth in Hz. This FoM, proposed in (Dong et al., 2023), balances multiple objectives for an OpAmp design.

Using an online approach, we aim to maximize the FoM. Since the performance of gradient ascent depends on the initial starting point, we first draw 500 random sizings uniformly from the allowed sizing ranges. In each iteration, we update the surrogate model by performing 100 epochs of supervised training on the available data. Then, we apply one step of gradient ascent using Adam on the 5 best samples, with gradients provided by the surrogate model. Overall, we do this for a total of 200 iterations.

Figs. 3d and e present the results for 200 randomly chosen initial points, where we also compare against a random baseline that selects 5 samples randomly within the allowed sizing ranges. Comparing the base model with the proposed locality-aware model, we observe that our method performs significantly better. This improvement is also evident in the results shown in Table 1. For example, using the gradient from our locality-aware model with 50 iterations yields better results than using the gradient from the base model with 200 iterations, indicating that we require far fewer active samples to be collected.

5.3. OWMS

Optical wave manipulation has numerous practical applications, ranging from imaging to the emerging field of optical neural networks, where light in optical setups is used for performing neural computation (Momeni et al., 2023a;b). A key component of such systems is the manipulation of optical waves using Spatial Light Modulation (SLM). The modulation of an input optical field, $\psi_{\text{in}}(x, y)$, by a complex-valued modulation profile \mathfrak{M} , is achieved as an elementwise product. The resulting output field $\psi_{\text{out}}(x, y)$, is expressed as

$$\psi_{\text{out}}(x, y) = \mathfrak{M} \cdot \psi_{\text{in}}(x, y). \quad (14)$$

The free-space propagation of optical fields between planes is modeled using scalar diffraction theory. According to the Rayleigh–Sommerfeld diffraction integral, the propagation of an input field $\psi_0(x', y')$ at $z = 0$ to a position (x, y, z) is given by

$$\psi_z(x, y) = \iint \mathfrak{h}_z(x - x', y - y') \psi_0(x', y') dx' dy'. \quad (15)$$

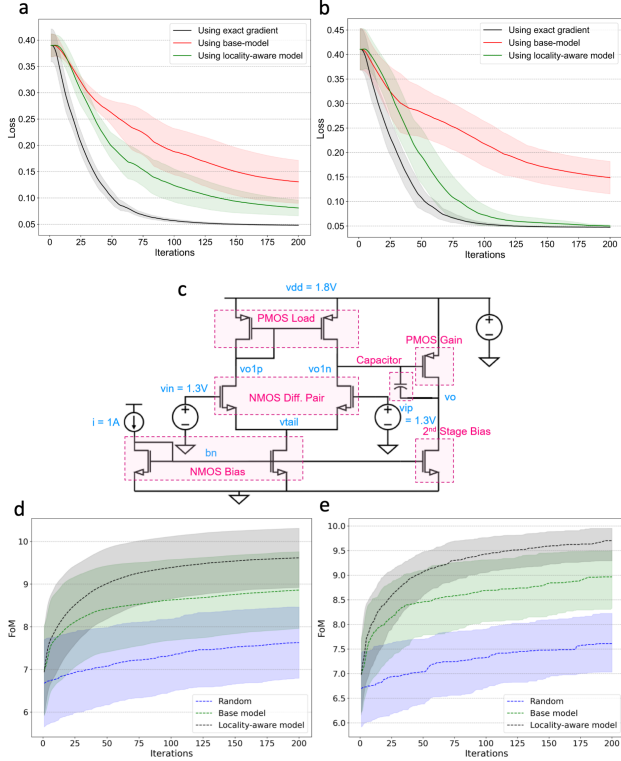


Figure 3. Performance of ABBO using the online-trained surrogate model for the CNON task ($\lambda = [-0.55, 0.125, 0.31, -0.38, 0.60]$): **a** without local sampling ($N_s = 0$) and **b** with local sampling ($N_s = 1$). **c** Schematic of the OpAmp circuit. **d** Mean \pm standard deviation and **e** median with interquartile range (IQR) of ABBO using the online-trained surrogate model for the OpAmp task.

Here, the impulse response h_z is expressed as

$$h_z(x - x', y - y') = \frac{z}{i\lambda\mathfrak{d}} \left(1 + \frac{i}{\mathfrak{d}} \right) \exp(i\mathfrak{k}\mathfrak{d}), \quad (16)$$

where $\mathfrak{d} = \sqrt{(x - x')^2 + (y - y')^2 + z^2}$ is the Euclidean distance between the input and output positions, λ is the wavelength, and $\mathfrak{k} = \frac{2\pi}{\lambda}$ is the wavenumber. We use TorchOptics (Filipovich & Lvovsky, 2024) to numerically evaluate the diffraction integral in (15) using the fast Fourier transform (FFT) by treating it as a convolution.

We consider a Gaussian beam as the input field, with a waist radius of $70 \mu\text{m}$ and a wavelength of 700 nm . The objective of the optimization is to determine the complex values of \mathfrak{M} such that the input Gaussian beam splits into two Gaussian beams at the output (see Fig. 4a). The dimension of \mathfrak{M} is 60×60 , resulting in a total of 3600 parameters to be optimized. We perform ABBO optimization by leveraging the fact that all computations for calculating the optical field and the objective function—defined as the difference in the ℓ_1 -norm between the target field and the output field, $\|\psi_{\text{out}}(x, y) - \psi_{\text{target}}(x, y)\|_1$ —are conducted through a black-box simulator implemented using TorchOptics. We also

Method	(1) CNON Task Budget $O(\cdot)$ to reach Base-model performance		Reduction Ratio
	$N_s = 0$	$N_s = 1$	
Locality-aware model	$O(100)$	$O(120)$	$\sim 50\%$ ($N_s = 0$) and $\sim 70\%$ ($N_s = 1$)
Method	(2) OpAmp Task Budget $O(\cdot)$ to reach Base-model performance		Reduction Ratio
	Locality-aware model	$O(1000)$	
Method	(3) OWMS Task Budget $O(\cdot)$ to reach Base-model/BayOpt performance		Reduction Ratio
	Locality-aware model	$O(750)/O(1200)$	

Table 2. Budget $O(\cdot)$ of black-box calls required for locality-aware models to match the performance of the Base-model or BayOpt after 200 iterations.

implement Random and BayOpt schemes under the same settings as those used for the base model and the locality-aware model, all evaluated over 100 randomly chosen initial points. The corresponding results, including the mean \pm standard deviation (std) and interquartile range (IQR) of the loss values, are presented in Figs. 4b and c, as well as in Table 1. The results show that the locality-aware model outperforms all the aforementioned approaches.

5.4. Discussion of the Results

We also implement another analysis on the number of black-box queries required by locality-aware models to match the performance of the base model or BayOpt after 200 iterations across all tasks (see Table 2). Notably, the reduction ratio exceeds 40% for all tasks, highlighting the effectiveness of our approach. From the results, we can conclude that using our proposed *GradPIE* loss allows to learn surrogate models with enhanced gradient estimation accuracy, which is critical for optimization tasks. These models are particularly effective in complex, high-dimensional systems (e.g., CNON and OWMS), where exact gradients are unavailable or computationally expensive to compute. There are some important points that need to be highlighted here.

First, as mentioned in the Appendix, simple multilayer perceptrons (MLPs) are used as surrogate models for learning gradients. However, other surrogate models that can be trained using *GradPIE* could also be employed to improve gradient estimation performance. For instance, generative adversarial networks (GANs) can be used for the same purpose (Shirobokov et al., 2020).

Second, in Algorithm 1, we employ a simple local sampling method, which involves sampling from a normal distribution around the newly updated input with a small standard deviation. However, more advanced methods could be utilized to generate local samples. For example, the Latin Hypercube Sampling (LHS) algorithm (Iman et al., 1980), which is well-suited for high-dimensional spaces, or approaches that

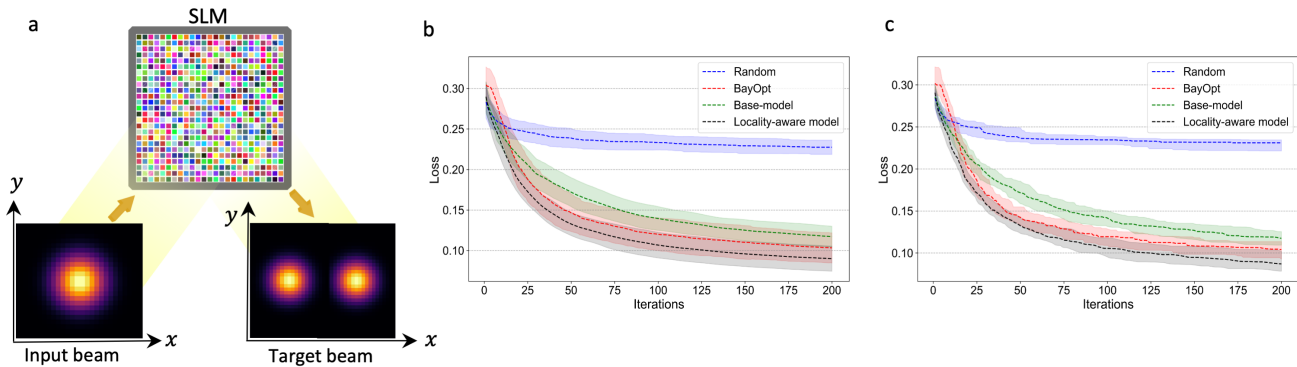


Figure 4. **a** Schematic of the OWMS. An input Gaussian beam is illuminated onto a Spatial Light Modulator (SLM) with 3600 parameters to be optimized such that the output waveform matches the target waveform. **b** Mean \pm standard deviation and **c** median with interquartile range (IQR) of ABBO using the online-trained surrogate model for the OWMS task.

leverage local gradient information to guide the sampling.

Third, the effectiveness of utilizing surrogate models to estimate gradients for gradient-based black-box optimization, compared to other methods such as numerical differentiation with gradient descent, guided evolutionary strategies, and BayOpt, has been demonstrated in previous studies (Grathwohl et al., 2017; Shirobokov et al., 2020; Ruiz et al., 2018; Louppe et al., 2019). Although we compared our performance with BayOpt and random search, a fair and rigorous comparison to verify the effectiveness of the proposed locality-aware surrogate model using the *GradPIE* loss function is to compare it with the exact same surrogate model trained with MSE or MAE loss functions, as demonstrated across all tasks.

6. Related Work

Several methods for black-box optimization exist, mainly differing in whether gradients of the objective function are available. In non-gradient-based optimization such as those modeled by Monte Carlo simulators, only data samples from an intractable likelihood can be generated. Common approaches in these cases include genetic algorithms (Banzhaf et al., 1998), BayOpt (Snoek et al., 2012; Eriksson et al., 2019), and numerical differentiation (Svanberg, 1987). However, these methods often lack scalability for high-dimensional black-box systems. Black-box gradient-based optimization methods can be broadly categorized into two classes: offline black-box optimization and active black-box optimization, depending on the system under optimization. In scenarios where actively querying the black-box function is impossible or challenging, offline black-box optimization is more suitable. Conversely, active black-box optimization is well-suited for scenarios compatible with automated *in silico* or *in situ* experimental settings, such as simulators, robotics, smart sensors, and the training of analog neural networks.

Offline black-box optimization A fundamental challenge in offline optimization lies in the mismatch between surrogate predictions and true objective values, particularly when extrapolating beyond training data. Conservative Objective Models (COMs) (Trabucco et al., 2021) address this by penalizing overestimations of out-of-distribution inputs through adversarial training. Building on this, (Fu & Levine, 2021) reduces prediction uncertainty via normalized data likelihood maximization. (Yu et al., 2021) adopts techniques in model pre-training and adaptation to enforce a criteria of local smoothness. Alternative strategies focus on the search process. They represent the search model as a distribution conditioned on the rare event of achieving high oracle performance or an adaptive gradient update policy with learnable parameters (Brookes et al., 2019; Fannjiang & Listgarten, 2020; Chemingui et al., 2024).

Active Black-Box Optimization Traditional ABBO methods rely on global surrogate models with BayOpt (Snoek et al., 2012) or stochastic gradient estimators (Wang et al., 2018) being predominant choices. While differentiable surrogates (Kumar & Levine, 2020; Eriksson et al., 2019) enable direct gradient-based optimization, they struggle with gradient misalignment in data-scarce regimes. Finite-difference approximations (Spall et al., 2022) provide alternative gradient estimates but become computationally prohibitive in high-dimensional spaces. The L-GSO framework (Shirobokov et al., 2020) trains deep generative models to iteratively approximate the simulator in local neighborhoods of the parameter space demonstrating improved sample efficiency for high-dimensional problems. Under limited query budgets, such methods often struggle to align the surrogate’s gradients with the exact gradients.

7. Conclusion

This study presents a novel theoretical framework for active gradient-based black-box optimization, focusing on enhancing gradient estimation through the use of locality-aware

surrogate models. Central to this framework is the proposed *GradPIE* loss function, which significantly improves gradient estimation for both offline and online training of surrogate models. Building on this theoretical foundation, we developed a novel algorithm for creating surrogate models exhibiting good gradient matching and by this achieving superior performance across diverse real-world benchmarks. While the proposed theory and algorithm are rooted in the domain of active gradient-based optimization, the underlying principles have broader applicability to related fields such as reinforcement learning.

Impact Statement

This paper introduces a novel theoretical perspective for understanding and analyzing gradient-based optimization problems through surrogate models, offering a cost-effective alternative to traditional gradient estimation via surrogate models. The methodological advancements and insights presented in this work have the potential to drive improvements across various science and engineering domains, well-suited for automated *in silico* or *in situ* experimental settings. In particular, the training of physical neural networks—analogue neural networks such as memristor-based (Yao et al., 2020; Aguirre et al., 2024) and optical neural networks (Ma et al., 2025; Bernstein et al., 2023)—has recently garnered significant attention due to their exceptional energy efficiency (McMahon, 2023; Momeni et al., 2023a). One of the most widely adopted approaches for training such networks involves the use of surrogate models to estimate gradients. We posit that the proposed algorithm can substantially enhance the training of such analogue neural networks, enabling more efficient and effective training schemes.

References

- Aguirre, F., Sebastian, A., Le Gallo, M., Song, W., Wang, T., Yang, J. J., Lu, W., Chang, M.-F., Ielmini, D., Yang, Y., et al. Hardware implementation of memristor-based artificial neural networks. *Nature communications*, 15(1): 1974, 2024.
- Ashby, M. Multi-objective optimization in material design and selection. *Acta materialia*, 48(1):359–369, 2000.
- Banzhaf, W., Nordin, P., Keller, R. E., and Francone, F. D. *Genetic programming: an introduction: on the automatic evolution of computer programs and its applications*. Morgan Kaufmann Publishers Inc., 1998.
- Bernstein, L., Sludds, A., Panuski, C., Trajtenberg-Mills, S., Hamerly, R., and Englund, D. Single-shot optical neural network. *Science Advances*, 9(25):eadg7904, 2023.
- Braun, O. M. and Kivshar, Y. S. Nonlinear dynamics of the frenkel–kontorova model. *Physics Reports*, 306(1-2): 1–108, 1998.
- Brookes, D., Park, H., and Listgarten, J. Conditioning by adaptive sampling for robust design. In *International conference on machine learning*, pp. 773–782. PMLR, 2019.
- Chemingui, Y., Deshwal, A., Hoang, T. N., and Doppa, J. R. Offline model-based optimization via policy-guided gradient search. In *Proceedings of the AAAI Conference on Artificial Intelligence*, volume 38, pp. 11230–11239, 2024.
- Dao, M. C., Le Nguyen, P., Truong, T. N., and Hoang, T. N. Boosting offline optimizers with surrogate sensitivity. In *Forty-first International Conference on Machine Learning*, 2024.
- de Avila Belbute-Peres, F., Smith, K., Allen, K., Tenenbaum, J., and Kolter, J. Z. End-to-end differentiable physics for learning and control. *Advances in neural information processing systems*, 31, 2018.
- Degrave, J., Hermans, M., Dambre, J., and Wyffels, F. A differentiable physics engine for deep learning in robotics. *Frontiers in neurorobotics*, 13:6, 2019.
- Dong, Z., Cao, W., Zhang, M., Tao, D., Chen, Y., and Zhang, X. Cktgnn: Circuit graph neural network for electronic design automation. *arXiv preprint arXiv:2308.16406*, 2023.
- Eriksson, D., Pearce, M., Gardner, J., Turner, R. D., and Poloczek, M. Scalable global optimization via local bayesian optimization. *Advances in neural information processing systems*, 32, 2019.
- Fannjiang, C. and Listgarten, J. Autofocused oracles for model-based design. *Advances in Neural Information Processing Systems*, 33:12945–12956, 2020.
- Filipovich, M. J. and Lvovsky, A. Torchoptics: An open-source python library for differentiable fourier optics simulations. *arXiv preprint arXiv:2411.18591*, 2024.
- Fu, J. and Levine, S. Offline model-based optimization via normalized maximum likelihood estimation. *arXiv preprint arXiv:2102.07970*, 2021.
- Grathwohl, W., Choi, D., Wu, Y., Roeder, G., and Duvenaud, D. Backpropagation through the void: Optimizing control variates for black-box gradient estimation. *arXiv preprint arXiv:1711.00123*, 2017.
- Hutter, F., Hoos, H. H., and Leyton-Brown, K. Sequential model-based optimization for general algorithm configuration. In *Learning and Intelligent Optimization: 5th*

- International Conference, LION 5, Rome, Italy, January 17-21, 2011. Selected Papers 5*, pp. 507–523. Springer, 2011.
- Iman, R. L., Davenport, J. M., and Zeigler, D. K. Latin hypercube sampling (program user’s guide).[lhc, in fortran]. Technical report, Sandia Labs., Albuquerque, NM (USA), 1980.
- Krishnamoorthy, S., Mashkaria, S. M., and Grover, A. Generative pretraining for black-box optimization. *arXiv preprint arXiv:2206.10786*, 2022.
- Kumar, A. and Levine, S. Model inversion networks for model-based optimization. *Advances in neural information processing systems*, 33:5126–5137, 2020.
- Lanthaler, S., Rusch, T. K., and Mishra, S. Neural oscillators are universal. *Advances in Neural Information Processing Systems*, 36, 2024.
- Louppe, G., Hermans, J., and Cranmer, K. Adversarial variational optimization of non-differentiable simulators. In *The 22nd International Conference on Artificial Intelligence and Statistics*, pp. 1438–1447. PMLR, 2019.
- Ma, S.-Y., Wang, T., Laydevant, J., Wright, L. G., and McMahan, P. L. Quantum-limited stochastic optical neural networks operating at a few quanta per activation. *Nature Communications*, 16(1):359, 2025.
- McMahan, P. L. The physics of optical computing. *Nature Reviews Physics*, 5(12):717–734, 2023.
- Mennel, L., Symonowicz, J., Wachter, S., Polyushkin, D. K., Molina-Mendoza, A. J., and Mueller, T. Ultrafast machine vision with 2d material neural network image sensors. *Nature*, 579(7797):62–66, 2020.
- Mohamed, S., Rosca, M., Figurnov, M., and Mnih, A. Monte carlo gradient estimation in machine learning. *Journal of Machine Learning Research*, 21(132):1–62, 2020.
- Momeni, A., Rahmani, B., Malléjac, M., Del Hougne, P., and Fleury, R. Backpropagation-free training of deep physical neural networks. *Science*, 382(6676):1297–1303, 2023a.
- Momeni, A., Rahmani, B., Malléjac, M., del Hougne, P., and Fleury, R. Phyff: Physical forward forward algorithm for in-hardware training and inference. In *Machine Learning with New Compute Paradigms*, 2023b.
- Nguyen, A. W. and Daugherty, P. S. Evolutionary optimization of fluorescent proteins for intracellular fret. *Nature biotechnology*, 23(3):355–360, 2005.
- Oguz, I., Dinc, N. U., Yildirim, M., Ke, J., Yoo, I., Wang, Q., Yang, F., Moser, C., and Psaltis, D. Optical diffusion models for image generation. *arXiv preprint arXiv:2407.10897*, 2024.
- Ruiz, N., Schuler, S., and Chandraker, M. Learning to simulate. *arXiv preprint arXiv:1810.02513*, 2018.
- Sarkisyan, K. S., Bolotin, D. A., Meer, M. V., Usmanova, D. R., Mishin, A. S., Sharonov, G. V., Ivankov, D. N., Bozhanova, N. G., Baranov, M. S., Soylemez, O., et al. Local fitness landscape of the green fluorescent protein. *Nature*, 533(7603):397–401, 2016.
- Shahriari, B., Swersky, K., Wang, Z., Adams, R. P., and De Freitas, N. Taking the human out of the loop: A review of bayesian optimization. *Proceedings of the IEEE*, 104(1):148–175, 2015.
- Shirobokov, S., Belavin, V., Kagan, M., Ustyuzhanin, A., and Baydin, A. G. Black-box optimization with local generative surrogates. *Advances in neural information processing systems*, 33:14650–14662, 2020.
- Si, Q., Yu, R., and Abrahams, E. High-temperature superconductivity in iron pnictides and chalcogenides. *Nature Reviews Materials*, 1(4):1–15, 2016.
- Snoek, J., Larochelle, H., and Adams, R. P. Practical bayesian optimization of machine learning algorithms. *Advances in neural information processing systems*, 25, 2012.
- Spall, J., Guo, X., and Lvovsky, A. I. Hybrid training of optical neural networks. *Optica*, 9(7):803–811, 2022.
- Svanberg, K. The method of moving asymptotes—a new method for structural optimization. *International journal for numerical methods in engineering*, 24(2):359–373, 1987.
- Trabucco, B., Kumar, A., Geng, X., and Levine, S. Conservative objective models for effective offline model-based optimization. In *International Conference on Machine Learning*, pp. 10358–10368. PMLR, 2021.
- Wang, Y., Du, S., Balakrishnan, S., and Singh, A. Stochastic zeroth-order optimization in high dimensions. In *International conference on artificial intelligence and statistics*, pp. 1356–1365. PMLR, 2018.
- Williams, R. J. Simple statistical gradient-following algorithms for connectionist reinforcement learning. *Machine learning*, 8:229–256, 1992.
- Williamson, R. E. and Trotter, H. F. *Multivariable Mathematics*. Pearson Prentice Hall, 4th edition, 2004.

Wright, L. G., Onodera, T., Stein, M. M., Wang, T., Schachter, D. T., Hu, Z., and McMahon, P. L. Deep physical neural networks trained with backpropagation. *Nature*, 601(7894):549–555, 2022.

Yao, P., Wu, H., Gao, B., Tang, J., Zhang, Q., Zhang, W., Yang, J. J., and Qian, H. Fully hardware-implemented memristor convolutional neural network. *Nature*, 577(7792):641–646, 2020.

Yu, S., Ahn, S., Song, L., and Shin, J. Roma: Robust model adaptation for offline model-based optimization. *Advances in Neural Information Processing Systems*, 34: 4619–4631, 2021.

Zheng, Z., Duan, Z., Chen, H., Yang, R., Gao, S., Zhang, H., Xiong, H., and Lin, X. Dual adaptive training of photonic neural networks. *Nature Machine Intelligence*, 5(10):1119–1129, 2023.

Zhou, F. and Chai, Y. Near-sensor and in-sensor computing. *Nature Electronics*, 3(11):664–671, 2020.

A. Appendix

Details of the CNON As mentioned in the main text (section 5.1), the CNON is described by (11). The coupling coefficients, \mathfrak{J}_{ij} , are symmetric. To enforce the condition, we construct \mathfrak{J}_{ij} from the relation:

$$\mathfrak{J}_{ij} = \frac{S + S^\top}{2}, \quad (\text{A1})$$

where \top represents the transpose operation. Here, S is an $N \times N$ matrix. For notational simplicity, we use a new matrix Q such that the off-diagonal elements of Q are identical to those of \mathfrak{J} , and the diagonal elements are given by:

$$Q_{ii} = -\sum_j \mathfrak{J}_{ij}. \quad (\text{A2})$$

Using this matrix, the equations of motion can be simplified into a matrix form:

$$\frac{d^2 \mathbf{q}_i}{dt^2} = -\sin(\pi \mathbf{q}_i) + \sum_{j=1}^N Q_{ij} \sin(\pi \mathbf{q}_j) + \mathbf{e}_i, \quad (\text{A3})$$

We use the 4th order Runge–Kutta (RK4) method to solve the aforementioned ODE.

The matrix Q_{ij} is set as $U_{ij} + Z_{ij}$, where U_{ij} and Z_{ij} are once matrix and a random matrix sampled from a uniform distribution in the range $[-1, 1]$, respectively. Similarly, $\mathbf{e}_i = Z_i$, where Z_i is a random vector sampled from a uniform distribution in the range $[-1, 1]$.

Details of the OpAmp For our experiments, we simulated the two-stage operational amplifier (OpAmp) using NGspice¹ and the Skywater-PDK² 130nm process. The parameter ranges for the transistors were set as follows: the width and length of the biasing transistors, differential pair, load transistors, and gain transistors were varied between 2 to 32 μm and 0.2 to 2 μm , respectively. The width of the second stage biasing NMOS is defined as integer multiple of the width of the first stage biasing NMOS. The ratio between these two values is chosen from 1, 2, 3. The value of the compensation cap was set between 0.1 pF and 20 pF.

Details of surrogate models We used simple MLP models as surrogate models for different tasks. Here, we provide the architecture of the MLP models in Table 3.

Table 3. Architecture of the MLP models used for the three tasks: CNON, OpAmp, and OWMS.

Task	Number of Hidden Layers	Size of Hidden Layers	Activation Function	Bias	Optimizer	LayerNorm
CNON	2	[256, 256]	GELU	Yes	Adam	No
OpAmp	4	[100, 100, 100, 20]	GELU	Yes	Adam	Yes
OWMS	5	[1000, 1000, 1000, 1000, 500]	GELU	Yes	Adam	Yes

¹<https://ngspice.sourceforge.io/>

²<https://github.com/google/skywater-pdk>

Algorithm A1 (Part A) Surrogate Training with *GradPIE* Loss, **(Part B)** Black-box Optimization via Trained Surrogate.

Input: Dataset $\mathcal{D} = \{(\mathbf{x}_i, \mathbf{y}_i)\}_{i=1}^N$, initial surrogate parameters θ , learning rates η_1 and $\eta_2 > 0$, number of epochs L_{epochs} , number of nearest neighbors K , black-box $\mathbf{F}(\cdot)$, number of optimization steps τ , convergence threshold ϵ

Output: Trained surrogate $\hat{\mathbf{F}}(\cdot; \theta)$, optimized input \mathbf{x}^*

Part A: Train the Surrogate Model.

Initialize θ ($\theta^{(0)} \leftarrow \theta$) and precompute \mathbf{x}'_k for each $\mathbf{x}_i \in \mathcal{D}$.

```

for  $l = 1$  to  $L_{\text{epochs}} - 1$  do
  foreach mini-batch  $\mathcal{B} \subseteq \mathcal{D}$  do
    | Compute  $\mathcal{L}_{\text{GradPIE}}$  using Eq. (10) for  $\mathcal{B}$ 
  end
   $\theta^{(l+1)} \leftarrow \theta^{(l)} - \eta_1 \nabla_{\theta} \mathcal{L}_{\text{GradPIE}}(\theta) \Big|_{\theta=\theta^{(l)}}$  // Update surrogate parameters
  if  $\mathcal{L}_{\text{GradPIE}} < \epsilon$  then
    | Break // Stop if loss converges
  end
end

```

Pass trained surrogate $\hat{\mathbf{F}}(\cdot; \theta)$ to Part B.

Part B: Optimization Loop.

Initialize $\mathbf{x} \sim \mathcal{N}(0, I)$ ($\mathbf{x}^{(0)} \leftarrow \mathbf{x}$).

```

for  $t = 1$  to  $\tau - 1$  do
  |  $\mathbf{x}^{(t+1)} \leftarrow \mathbf{x}^{(t)} - \eta_2 \nabla_{\mathbf{x}} \hat{\mathbf{F}}(\mathbf{x}; \theta)$  // Perform gradient descent on  $\mathbf{x}$  using surrogate gradients
end

```

Return: optimized input \mathbf{x}^* .
